Correspondence to:
N. Sakaeda,
nsakaeda@ou.edu

The Observed Effects of Cold Pools on Convection Triggering and Organization During DYNAMO/AMIE

Naoko Sakaeda[1] and **Giuseppe Torri[2]**

[1]School of Meteorology, University of Oklahoma, Norman, OK, USA, [2]Department of Atmospheric Sciences, University of Hawai'i at Mānoa, Honolulu, HI, USA

Abstract Cold pools that form from existing convection can generate new clouds nearby, a process that has been suggested to contribute to cloud organization. However, some disagreement exists on the role of cold pools in cloud organization over tropical oceans, and much remains to be understood on how this role depends on the state of large-scale disturbances such as the Madden-Julian Oscillation (MJO). This study addresses this question by examining the intraseasonal variability in the properties of cold pools and their effects on convection triggering using observations. The unique set of surface meteorology data and ground-based radars deployed during the DYNAMO/AMIE field campaign are used to identify cold pools and the associated spatiotemporal evolution of rainfall. The results suggest that cold pools enhance rainfall at their expected speed of 3–8 m s^{-1}, which includes the Doppler-shifting effect by the background wind. The cold pools also enhance rainfall mainly within a 20 km radius, especially in the direction of boundary-layer vertical wind shear. However, gravity waves appear to contribute predominantly to the propagation of convection over a wider range of distances due to their faster propagation speeds. The interface of convection triggering and propagation at different speeds of cold pools and gravity waves seems to contribute to cloud organization. The effectiveness of cold pools and gravity waves on cloud organization also depends highly on the MJO due to the combined effects of changes in environmental humidity and boundary to lower-tropospheric wind.

Plain Language Summary High-density air that forms due to evaporative cooling of rainfall and downward injection of colder air aloft spreads horizontally, a phenomenon known as a cold pool. The spreading edges of cold pools initiate new cumulus clouds by lifting humid air, which is thought to cluster cumulus clouds that can merge and form larger clouds. However, the importance of cold pools in cloud clustering remains debated. This study uses a unique combination of observational data collected during a field campaign deployed over the Indian Ocean to examine the effect of cold pools on cloud clustering. The results provide observational evidence that cold pools support cloud formation within a 20 km radius of the identified cold pools, helping the clustering of clouds within a limited distance. In addition to cold pools, gravity waves that form from cumulus clouds mainly lead to the propagation and formation of cumulus clouds over longer distances due to their faster propagation speeds. The formation of cumulus clouds over a varying range of distances due to different propagation speeds of cold pools and gravity waves seems critical to the clustering of clouds. However, their effectiveness on cloud formation depends on atmospheric conditions set by intraseasonal variability.

1. Introduction

Cold pools that form in the subcloud layer through rain evaporation and downdrafts of lower equivalent potential temperature from aloft are known to trigger new convection and lead to clustering of convection (e.g., Feng et al., 2015; Rowe & Houze, 2015; Schlemmer & Hohenegger, 2014; Torri & Kuang, 2019; Zuidema et al., 2017). This clustering of deep convection is one of the typical definitions of "cloud organization" that plays an important role in the global energy and water cycle (e.g., Retsch et al., 2020; Tobin et al., 2012; Tompkins & Semie, 2017). While it is important to improve our understanding of the processes involved in cloud organization, including those related to cold pools, capturing organization in numerical models remains an outstanding challenge (Moncrieff, 2019; Yang et al., 2019). Over the tropical ocean, large-scale disturbances, such as the Madden-Julian Oscillation (MJO), influence cloud organization (Sakaeda & Torri, 2022). However, how cold pools contribute to the intraseasonal variability of cloud organization is less understood, especially in observational studies. Changes in the large-scale environment are expected to affect the characteristics of cold pools (Schlemmer & Hohenegger, 2014), and therefore, cold pools may play different roles in cloud organization depending on the state of the MJO. The objective of this study is to use the observational data from the Dynamics of the

MJO/Atmospheric Radiation Measurement MJO Investigation Experiment (DYNAMO/AMIE) field campaign (Yoneyama et al., 2013) to examine how cold pool characteristics and their contributions to cloud organization vary with the MJO.

While the identification of cold pools is challenging from observations, de Szoeke et al. (2017) have demonstrated how surface station data could be used to identify cold pools from the Research Vessel (R/V) *Roger Revelle* during DYNAMO/AMIE. In particular, they showed that rainfall is often associated with the passages of cold pools, and the number of cold pools is higher during the enhanced phase of the MJO, while stronger cold pools can be observed during the MJO suppressed phase. These changes in the number and the properties (e.g., intensity) of cold pools may change the effectiveness of cold pools to generate new convection. For example, increased moisture at cold pool fronts is thought to provide thermodynamic forcing to convection triggering from simulations (Böing et al., 2012; Falk & van den Heever, 2023; Khairoutdinov & Randall, 2006; Schlemmer & Hohenegger, 2014; Tompkins, 2001a; Torri & Kuang, 2019). This moisture enhancement is also documented with the observed cold pools, although the observed magnitudes are smaller than simulations, and it occurs at the outer edge of cold pool fronts rather than within them (Chandra et al., 2018; de Szoeke et al., 2017; Zuidema et al., 2017). The magnitude of this thermodynamic forcing may also depend on the state of the MJO due to its associated changes in surface fluxes and environmental moisture that can be entrained into cold pools (Adames & Wallace, 2015; Sobel et al., 2014).

The changes in the number and properties of cold pools may support the increased clustering of convection during the MJO enhanced phase (Sakaeda & Torri, 2022). The increased number of cold pools may lead to their more frequent collisions, enhancing the mechanical forcing of convection triggering. Simulations have shown that these intersections of cold pool fronts are associated with stronger lifting, as well as wider, deeper, and stronger moisture anomalies that lead to more effective generating of deep convective clouds (Böing et al., 2012; Feng et al., 2015; Meyer & Haerter, 2020; Torri et al., 2015). Feng et al. (2015) also suggested that these cold pool intersections occur in regions of clustered (closely distanced) clouds that sustain a moist environment, supporting the development of deep clouds by reducing the entrainment of dry air. As the MJO transitions to its enhanced phase, the number of convective clouds increases, and their cold pools may collide more frequently to trigger convection, leading to the organization of clouds. Using S-PolKa radar data during DYNAMO/AMIE, Rowe and Houze (2015) showed that isolated convective cells form new clouds at the boundaries of their cold pools, helping the transition of shallow-to-deep convection toward the MJO enhanced phase. However, their approach was limited to identifying cold pools during the suppressed phase of the MJO.

While the prior results collectively support the idea that cold pools are important contributors to cloud organization, a detailed understanding of how they support intraseasonal cloud organization remains to be achieved, especially from observational studies. The importance of cold pools on cloud clustering over tropical oceans is also debated by Grant et al. (2018), who showed that stronger cold pools suppress convection by leading to more entrainment of less buoyant air, and gravity waves are more important to cloud organization. Some studies also suggest that cold pools are less important to cloud organization in the presence of widespread stratiform rain during the MJO enhanced phase (Chandra et al., 2018; Cheng et al., 2020). To provide insights into the role of cold pools, our study will focus on examining the behaviors and the roles of the interactions between cold pools and the large-scale environment in supporting cloud organization associated with the MJO. We address the following specific questions using data collected during DYNAMO/AMIE over the Indian Ocean.

1. How do the characteristics of cold pools vary with MJO phase?
2. How do the cold pools contribute to the organization of convection at varying stages of the MJO?

2. Data and Methods

We use data collected at Addu Atoll and from the *Revelle* during the DYNAMO/AMIE field campaign to identify cold pools and their impact on cloud organization from October 2011 to January 2012. During this period, three MJO events and a total of over 600 cold pools are identified at the two locations. The identification methods of cold pools and the MJO are described below. At these locations, surface measurement stations and radars were deployed in close proximity, allowing the examination of the spatiotemporal evolution of rainfall relative to the identified cold pools. We analyze both locations to increase our sample size and to test the sensitivity of results to the presence of islands. While the islands that form Addu Atoll are small (about 2–6 km^2) and are surrounded
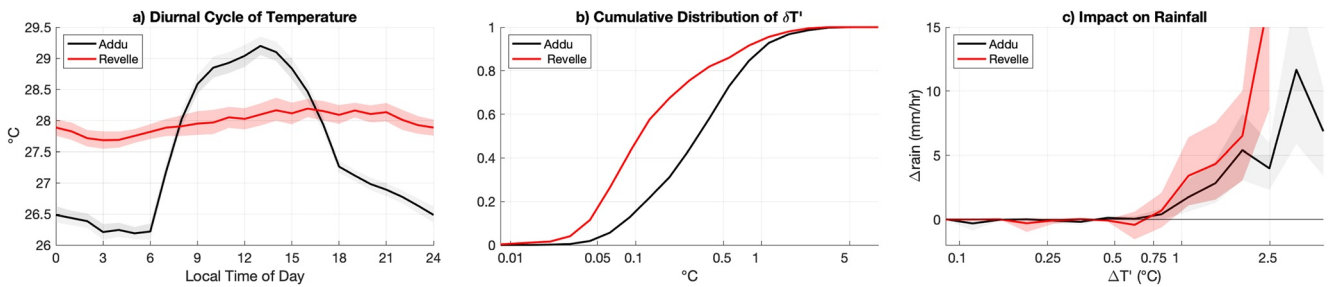
Figure 1. (a) Average hourly time series of surface temperature based on the local solar time (°C). (b) Cumulative distribution of the magnitude of all identified temperature drops near the surface ($\delta T'$, °C). (c) Change in rainfall before and after the identified temperature drops (mm hr^{-1}), stratified by the magnitudes of the temperature drops (see text for more detail). Black lines in all panels show Addu Atoll, and the red lines show the *Revelle*. Shadings show the 95% confidence interval.

by open ocean, the effects of the island on temperature, moisture, and winds are seen near the surface (Ciesielski & Johnson, 2021).

2.1. Cold Pool Identification

Cold pools are identified using 1-min surface temperature data measured by ARM Mobile Facility (AMF2) deployed over Gan Island of Addu Atoll and by the NOAA Earth System Research Laboratory Physical Sciences Division on the *Revelle*. Both data provide time series of near-surface air temperature data that are used to identify cold pools following the method of de Szoeke et al. (2017), which searches for continuous decreases in temperature. While no clear diurnal cycle of temperature appears at the *Revelle*, a strong diurnal cycle appears over Addu Atoll (Figure 1a). This strong diurnal cycle can result in false identification of cold pools, especially during the afternoon, when the temperature cools. To eliminate these false detections, we apply the method of de Szoeke et al. (2017) to the temperature anomalies, T', after eliminating the diurnal cycle by removing 3-hr triangular moving averages.

In brief, the method of de Szoeke et al. (2017) first applies an 11-min centered triangular window to generate low-pass temperature anomalies, and their continuous drops are identified as potential cold pools. The magnitude of the temperature drop is measured as the difference between the maximum and minimum values of temperature anomalies associated with each temperature drop. Using the notation of de Szoeke et al. (2017), the magnitude of low-pass temperature drop is noted as $\delta T'$, defined as the difference between the maximum low-pass temperature within 20 min of the start of the continuous temperature drop and the minimum low-pass temperature at the end of the temperature drop. The starting and ending times of the temperature drop are defined using the unfiltered temperature anomalies. The end of the temperature drop is the time of associated minimum unfiltered temperature anomalies t_{min}. The start of the temperature drop is the time of maximum unfiltered temperature anomalies, referred to as t_{max}. The temperature difference between the unfiltered temperature anomalies between t_{max} and t_{min} is defined as $\Delta T'$. We also check if the temperature without the removal of 3-hourly moving averages decreases over the duration of the continuous drop in temperature anomalies. Any events with an increasing trend in temperature are discarded as those are unlikely to be cold pools.

In de Szoeke et al. (2017), a low-pass temperature drop (δT) with a magnitude greater than 0.7°C is identified as a cold pool. We must first re-evaluate the appropriateness of using the same threshold because de Szoeke et al. (2017) did not remove 3-hr centered averages, and they did not identify cold pools at Addu Atoll. Figure 1b shows that the magnitudes of temperature drops are stronger over Addu Atoll than at the *Revelle*. Chandra et al. (2018) also find this difference, which they attribute to the existence of stronger and deeper clouds around Addu Atoll that may be associated with stronger downdrafts. We speculate that this difference in cold pool strength could also be due to the thermal gradient between the island and the surrounding ocean during the daytime. Due to the small area of Addu Atoll, nearly all identified cold pools are expected to originate from the surrounding ocean, which may result in a greater temperature drop over the island as the cold pools arrive. In fact, we find that the frequency and magnitude of cold pools are higher during the day than at night at Addu Atoll (not shown). This afternoon peak in the frequency of cold pools is also found by Garg et al. (2021) based on their cold pools that are identified from buoys in global ocean basins.

To determine an appropriate magnitude threshold to identify cold pools at each location, temperature drops are stratified by their magnitudes ($\delta T'$), and their impact on rainfall is examined. For each temperature drop, the

difference in the average rain gauge-measured rainfall 30 min before and after t_{max} is used to estimate their impact on rainfall. Figure 1c shows the averages of such impact conditioned by $\delta T'$. A positive rainfall difference indicates that rainfall increases after t_{max}. At both locations, temperature drops with magnitudes greater than 0.75°C tend to enhance rainfall, but the enhancement is more pronounced at the *Revelle* for strong temperature drops. This may be partly due to the smaller number of samples at the *Revelle* and a difference in the strength of gust front associated with cold pools. Prior studies show that an increase in wind speed (gust front) associated with cold pools is greater at the *Revelle* than at Addu Atoll (Chandra et al., 2018; Zuidema et al., 2017). We suspect that the presence of the Addu Atoll weakens the gust front and the associated mechanical forcing of cold pools to generate new convection over Addu Atoll. Although the exact reason for this difference in rainfall enhancement between the *Revelle* and Addu Atoll is unclear, Figure 1c suggests that we can use the same threshold of 0.7°C of $\delta T'$ as in de Szoeke et al. (2017) to identify cold pools at both locations because those events tend to be associated with expected rainfall enhancement from cold pools. We provide further analysis of rainfall triggering by cold pools in Sections 3 and 4 to examine their contribution to cloud organization.

In our analysis, we further restrict the number of cold pools at the *Revelle* to those that occur on days when the ship was considered stationary, located within a 1° box centered on 0°N and 80.5°N, and when the radar was operating (4–28 October, 11 November–2 December). This is done to eliminate potential biases in the identification of cold pools due to ship movement relative to cold pools. The ship was considered stationary when it was moving at a speed less than 10 km hr^{-1}, which corresponds to a documented speed of cold pool propagation (~3 m s^{-1}, Grant et al., 2018; Torri & Kuang, 2019). At Addu Atoll, all cold pools identified during the operation of the S-PolKa radar are used (1 October–15 January). This method identifies a total of 116 and 530 cold pools at the *Revelle* and Addu Atoll, respectively. The number of identified cold pools at the *Revelle* is smaller than de Szoeke et al. (2017) because of our elimination of cold pools while the ship was moving at a faster speed.

We use the same definitions of cold pool properties as in de Szoeke et al. (2017) to examine their variability with MJO phase. The intensity of cold pools is defined by the difference in maximum and minimum temperature anomalies ($\Delta T'$). Duration is defined as the time between t_{min} and t_{max}, representing the duration of the cold pool fronts. Recovery time is defined as the time it takes for the low-pass filtered temperature to increase for $\Delta T'/e$ from its minimum.

2.2. Ground-Based Radars and CombRet Product

We use ground-based scanning radars to examine the spatiotemporal evolution of rainfall relative to the identified cold pools. Over Addu Atoll, we use S-PolKa, which was deployed 8.62 km northwest of AMF2. S-PolKa is a polarimetric, dual-wavelength radar with S-band and Ka-band, that performed combined full horizontal scans with some vertical cross-section scans toward the location of AMF2. These scans were repeated on a 15-min cycle from 1 October 2011–15 January 2012. A NASA TOGA C-band radar onboard the *Revelle* also operated combined full horizontal scans and some vertical scans at a 10-min cycle between 1 October 2011 and 08 December 2011.

Near-surface rain rates are estimated from reflectivity for single-polarization C-band radars, while the relationships with differential reflectivity and derived specific differential phase from Thompson et al. (2018) are used for dual-polarization S-PolKa radar. In addition to rain rate estimates, the algorithm of Powell et al. (2016) is applied to classify rain types. Rainfall is classified into deep convective, stratiform, mixed (both deep convective and stratiform), isolated convective core and fringes, and weak echo based on the intensity and horizontal extent of echo interpolated to 2.5 km MSL at 1-km horizontal grids. This interpolation generates continuous data despite the fact that some beam blockage was noted to the west of the S-PolKa at a low elevation scan (Powell et al., 2016). Further descriptions of the methods of estimating rain rates and rain types are provided by Dolan et al. (2017). Both radars had a maximum range of 150 km. However, rain rate estimates are not available near the radar where the echo remains below 2 km, leading to the gap of rainfall information within 5–10 km of the radar that overlaps with the location of surface measurement stations (the locations of cold pool identification).

To complement this limitation of the radar data, we also use the Pacific Northwest National Laboratory (PNNL) Combined Remote Sensor retrieval algorithm (CombRet) product to study the evolution of precipitating cloud types at Addu Atoll. The CombRet data combine the AMF2 vertically pointing Doppler radar (KAZR), lidar retrievals, and S-PolKa reflectivities to identify cloud layers and their microphysical properties at a 30-s interval

(Feng et al., 2014). Following Feng et al. (2014), the precipitating clouds are defined to have cloud base below 3 km. Among those precipitating clouds, the ones with cloud top below 3 km are defined as shallow, 3–8 km as congestus, and above 8 km as deep clouds. This cloud classification method is different from the radar due to the lack of spatial information in the CombRet, but it provides additional data to examine cloud evolution relative to the occurrence of cold pools at Addu Atoll, where rain estimates from S-PolKa are not available.

The effects of large-scale circulation associated with the MJO on cold pools and cloud organization are tested using the Colorado State University surface and upper-air gridded data (Ciesielski et al., 2014). Both Addu Atoll and the *Revelle* had radiosonde launches that are included to generate this data set that include 3-hourly thermo-dynamic and kinematic variables at 1° horizontal and 25 hPa vertical grids. We mainly use these data to quantify the large-scale humidity, horizontal winds, and their vertical wind shear that have been suggested to be important to convection triggering by cold pools (Feng et al., 2014; Rotunno et al., 1988; Rowe & Houze, 2015).

2.3. Identification of MJO Phase

The state of MJO convective envelopes is identified locally, based on MJO-filtered Outgoing Longwave Radiation (OLR) anomalies at Addu Atoll and the *Revelle*. Twice daily, 2.5° gridded OLR data from 1979 to the present are obtained from NOAA Physical Sciences Laboratory (Liebmann & Smith, 1996). After removing the time average and the first three harmonics of the seasonal cycle from OLR, the inverse transform of Fourier coefficients is applied to filter for MJO wavenumber-frequency band (20–100 days and 1–5 eastward propagating wavenumbers), following the method of Wheeler and Kiladis (1999). This MJO-filtered OLR anomaly is averaged within a 5° box centered around Addu Atoll (2.5°N–2.5°S, 70–75°E) and the *Revelle* (2.5°N–2.5°S, 77.5–82.5°E). These time series of MJO-filtered OLR anomaly and their time tendencies are used to define the phase angle, which indicates the local state of MJO convection.

Figure 2a shows the evolution of MJO convection around Addu Atoll and the *Revelle* on this local MJO phase diagram. The local phase angles are defined in the same manner as Sakaeda and Torri (2022), where 0° indicates the center of the enhanced MJO convective envelope, and ±180° is the center of the suppressed convective envelope. A negative phase angle around −90° represents the developing state of enhanced convection (ahead or east of enhanced convection), and a positive phase angle around 90° represents its decaying state (behind or west of enhanced convection). Table 1 summarizes the dates that correspond to the centers of suppressed, developing, enhanced, and decaying phases of the MJO. These dates generally match the previously identified states of the MJO (e.g., Rowe & Houze, 2015; Sakaeda et al., 2018; Xu & Rutledge, 2015). The local evolution of MJO convection is similar at Addu Atoll and the *Revelle*, except that it is shifted by a few days, as expected.

This local MJO index allows us to easily compare the evolution of cold pools and clouds at these two stations. As an example, Figure 2b shows the composite of total OLR anomalies based on this local MJO phase at Addu Atoll and the *Revelle*. At both locations, the minimum OLR anomaly slightly lags the local phase 0° due to the persistence of high clouds after the time of peak precipitation (Kiladis et al., 2005).

2.4. Statistical Significance Test

Throughout the manuscript, all statistical significance is tested using a 1000-iteration bootstrap resampling with repetition and 95% confidence level. Using the bootstrap method, we find the confidence interval of the quantity that we want to test. This confidence interval is compared with the confidence interval of the null value, which is found by repeating the same analysis using randomly selected times. For example, if we want to test whether the intensity of cold pools during one phase of the MJO is significantly different from other phases of the MJO, then we randomly select cold pools from any phase of the MJO to generate the null value. An iteration of this random selection generates the confidence interval of the null value. When these two confidence intervals do not overlap, the difference is considered statistically significant.

3. Observed Intraseasonal Evolution of Cold Pools

We first show how the characteristics and frequency of cold pools vary with the MJO. de Szoeke et al. (2017) showed that the frequency of cold pools doubles from the suppressed to the enhanced phase of the MJO at the *Revelle*. However, we demonstrate that this result does not hold true at Addu Atoll.
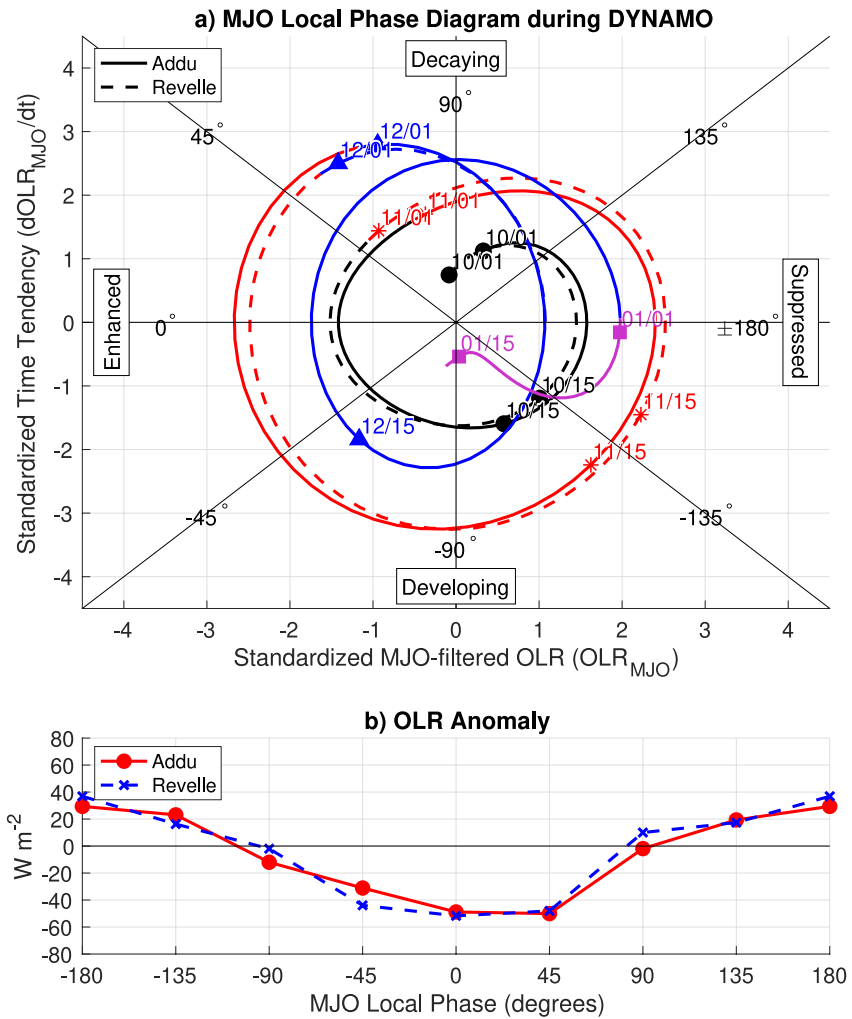
Figure 2. (a) Madden-Julian Oscillation (MJO) local phase diagram at Addu Atoll (solid line) and the *Revelle* (dashed line) based on MJO-filtered Outgoing Longwave Radiation (OLR) anomalies around each location (see text for more detail). The dates are shown on every 1st and 15th of each month. (b) Composites of total OLR anomalies with respect to MJO local phase.

Figure 3 shows that, despite the similar evolution of rainfall, the MJO appears to impact the frequency of cold pools differently at these two locations. At both locations, rainfall maximizes slightly before the center of the MJO enhanced convective envelopes (MJO local phase −45°), and it is mostly contributed by deep convective and stratiform rain (Figures 3a and 3b). At the *Revelle*, this rainfall variability aligns with the frequency of cold pools, which is about twice as high within the enhanced phase of the MJO than the suppressed phase (Figure 3d),

| Table 1				
Dates Corresponding to the Selected Madden-Julian Oscillation Local Phase				
MJO local phase	±180° suppressed	−90° developing	0° enhanced	90° decaying
Addu Atoll	9 October 2011	17 October 2011	25 October 2011	2 November 2011
	11 November 2011	18 November 2011	25 November 2011	3 December 2011
	7 December 2011	12 December 2011	18 December 2011	24 December 2011
	1 January 2012	15 January 2012		
Revelle	11 October 2011	19 October 2011	27 October 2011	2 October 2011
	13 November 2011	20 November 2011	27 November 2011	4 November 2011
	8 December 2011	13 December 2011	20 December 2011	4 December 2011
	2 January 2012			26 December 2011
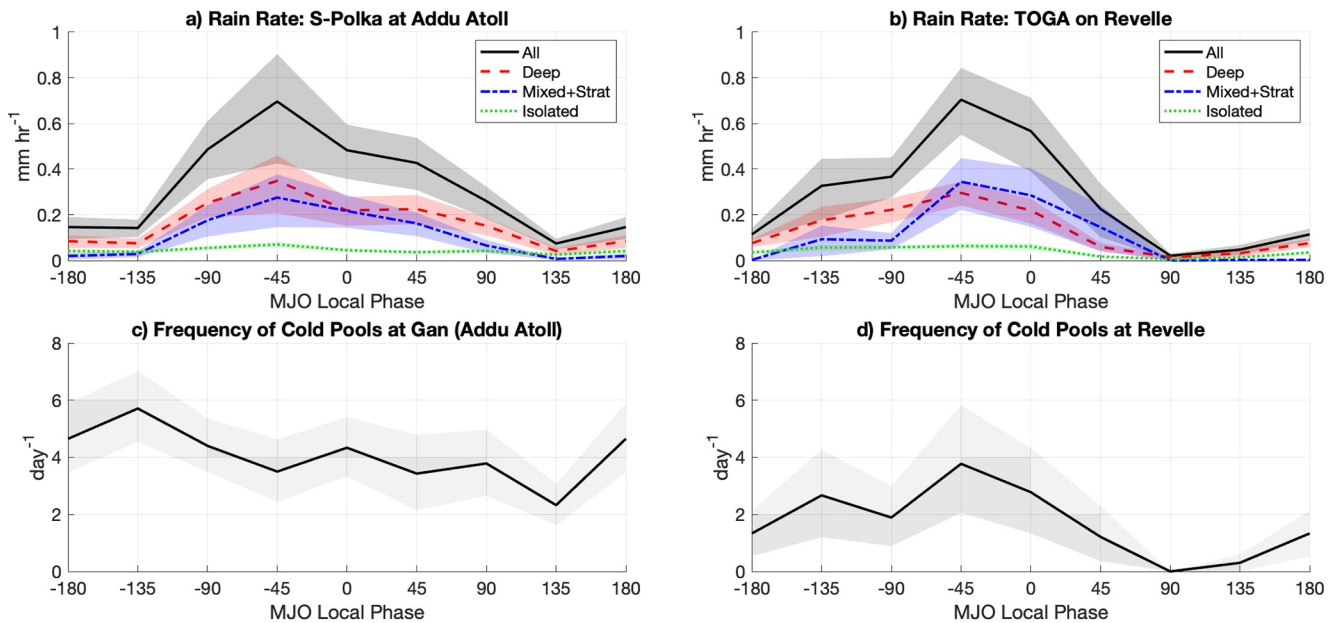
Figure 3. (a and b) Composites of domain-averaged rain rates from (a) S-PolKa at Addu Atoll and (b) TOGA radar on the *Revelle* based on Madden-Julian Oscillation local phase (mm hr^{-1}). Total rain (solid black) is separated into deep convective rain (dashed red), the sum of stratiform and mixed stratiform/deep convective rain (dot-dashed blue), and isolated rain (dotted blue). (c and d) Frequency of identified cold pools at Addu Atoll and the *Revelle* (number per day). Shadings around the lines show the 95% confidence interval.

consistent with the finding of de Szoeke et al. (2017). This increased frequency could be attributed to the increased number and intensity of deep convective cells that generate cold pools during the MJO enhanced phase. Sakaeda and Torri (2022) showed that the number of deep convective cells peaks with their domain-averaged rainfall from the S-PolKa data at Addu Atoll, and this is true at the *Revelle* as well (not shown). However, at Addu Atoll, the frequency of cold pools shows less fluctuation with the MJO, and it tends to be higher near the suppressed phase of the MJO (MJO local phase −135°) when the rainfall is at its minimum (Figure 3c). This indicates that the increased number of deep convective cells does not necessarily lead to an increased number of cold pools.

We speculate that this discrepancy in the intraseasonal evolution of cold pool frequency between the *Revelle* and Addu Atoll relates to different rainfall properties at these two locations. To investigate this hypothesis, we examine the relationship between the daily number of deep convective cells, the areal fraction of stratiform rain observed from S-PolKa and TOGA radars within a range of 50 km, and the number of cold pools (Figures 4a and 4b). We eliminate rainfall properties from a greater range that are unlikely to be directly related to the identified cold pools. Deep convective cells are identified as contiguous areas of raining pixels classified as "deep convection" through the algorithm of Powell et al. (2016), which can be embedded within wide-spread stratiform rain or within isolated, smaller raining systems. Days in the MJO enhanced (local phase ≥−45° and ≤45°) and suppressed phase (local phase ≤−135° or ≥135°) are indicated with triangles and upside-down triangles, while other days are indicated with circles. Both locations show that the increase in the number of deep convective cells is generally associated with the increased amount of stratiform rain (Powell, 2016; Sakaeda et al., 2018; Xu & Rutledge, 2014).

On days when the areal fraction of stratiform rain is below 0.2, a higher number of cold pools is associated with days with a higher number of deep convective cells at Addu Atoll and the *Revelle* (Figures 4a and 4b). This supports the prior findings that cold pools are more effective at supporting convection development when there is less widespread stratiform rain (Chandra et al., 2018; Cheng et al., 2020). However, the frequency of cold pools varies differently with the areal fraction of stratiform rain between the two locations. While a high frequency of cold pools occurs on days when the stratiform rain fraction is at the highest (i.e., MJO enhanced phase) at the *Revelle*, cold pool frequency is low on high-stratiform days at Addu Atoll, leading to the different intraseasonal evolutions of cold pool frequencies shown in Figure 3.

This discrepancy in the relationships between stratiform rain and cold pool frequency at the two locations seems to appear from the location of the deep convective cells relative to where the cold pools are identified. Figures 4c and 4d show the difference in spatial distribution of the deep convective cells between the days of MJO enhanced
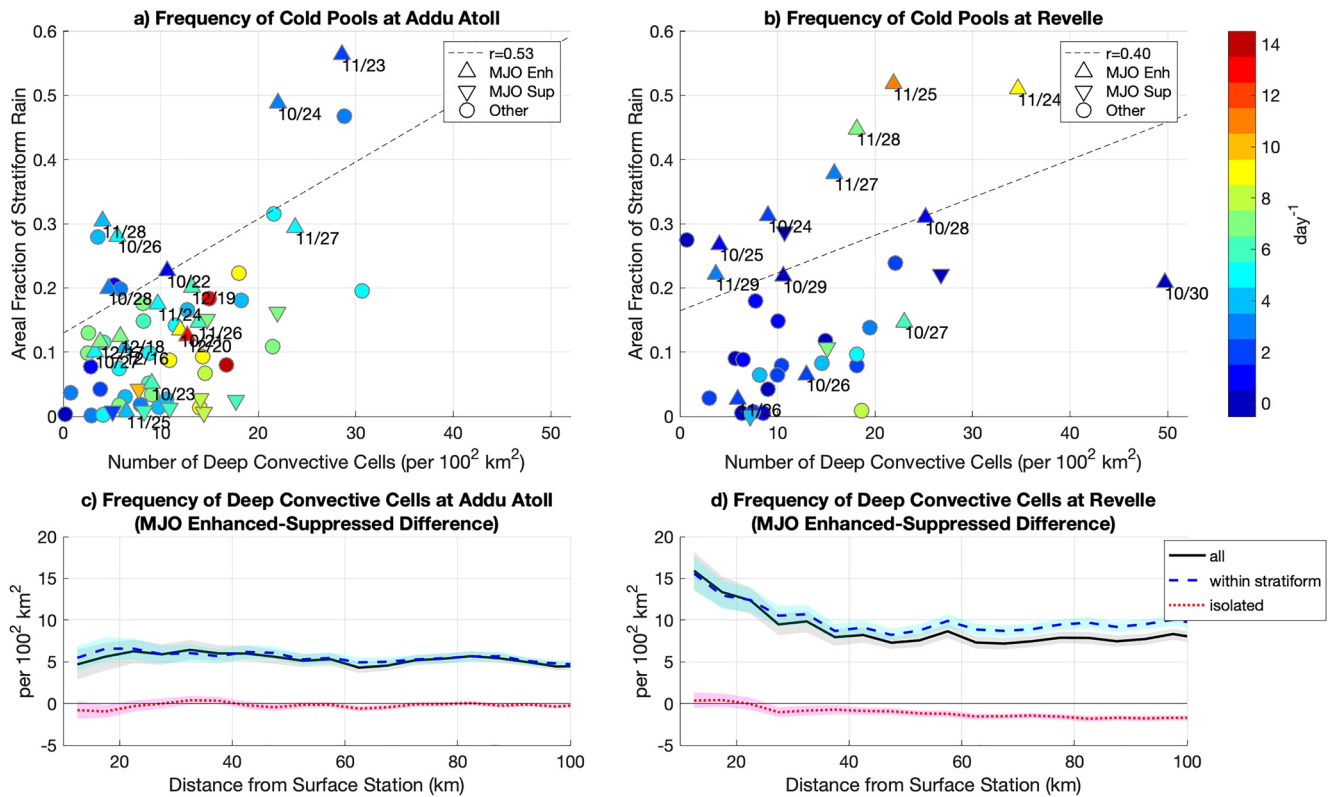
Figure 4. (a and b) Scatter plots of the daily number of deep convective cells (number per 100^2 km^2) and the areal fraction of stratiform rain observed by (a) S-PolKa and (b) TOGA radars within 50 km of their range. The dashed line shows the best-fit line and *r* value in the legend shows the correlation coefficient of the quantities on horizontal and vertical axes. Days within the Madden-Julian Oscillation (MJO) enhanced and suppressed phases are shown with triangles and upside-down triangles, respectively, while other days are shown with circles. Shadings of these markers show the frequency of identified cold pools (number per day) at each location. (c and d) Difference in the frequency of deep convective cells between the MJO enhanced and suppressed phases as a function of distance from surface measurement station (the location of identified cold pools) in black line, separated into ones embedded within stratiform (dashed blue) and isolated rain (dotted red). Shadings around the lines show the 95% confidence interval.

and suppressed phase from each location. At both locations, deep convective cells become more frequent during the MJO enhanced phase, especially the ones embedded within stratiform rain. While this happens uniformly in space around Addu Atoll, at the *Revelle*, deep convective cells become more concentrated at distances close to the surface measurement station (within 40 km), where the cold pools are identified in this study.

This occurrence of convective rain closer to the surface station on the *Revelle* may have led to the observed higher frequency of cold pools within the MJO enhanced phase. Given that there is no physical reason why convective cells should form more frequently near the *Revelle*, this might have occurred by a random chance or due to a greater error in rainfall estimates from C-band radar, especially at its longer range. In addition, the 3 days with above 0.4 stratiform rain fraction at the *Revelle* that had high cold pool frequencies occurred during the November MJO event, biasing the results. This behavior of the November MJO event also contradicts prior findings (Chandra et al., 2018; Cheng et al., 2020), which suggest that the widespread stratiform rain produces broad areas of cool near-surface temperature through rain evaporation and weakens cold pools and their effects on convection development. Therefore, the observed high frequency of cold pools during the November MJO event at the *Revelle* might be an outlier. The relationship between cold pool frequency and the MJO seen in Figure 3d and in de Szoeke et al. (2017) at the *Revelle* might not be applicable to all MJO events, and an increased sampling is needed to confirm their relationship.

In addition to cold pool frequency, we detect no statistically robust variability in other cold pool properties with the MJO. Figure 5 shows the probability distribution of cold pool magnitude, duration, and recovery times at different local phases of the MJO. At both locations, these quantities tend to peak around the MJO enhanced phase, but no statistical significance is found. de Szoeke et al. (2017) also find no significant correlation between
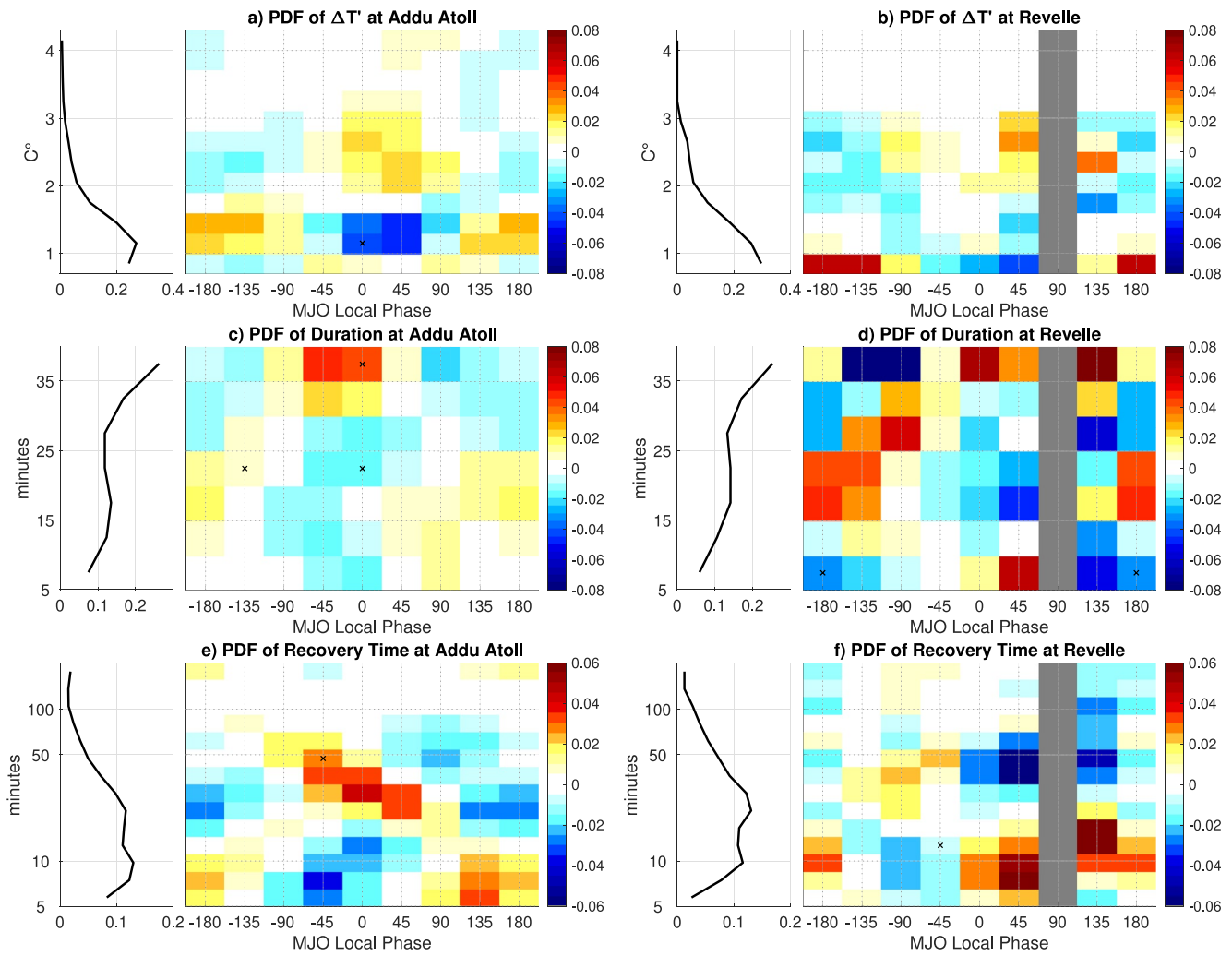
Figure 5. Probability distributions of cold pool (a and b) intensity ($\Delta T'$, C°), (c and d) duration of its front (minutes), (e and f) recovery time (minutes). The left column shows Addu Atoll, and the right column shows the *Revelle*. Black lines on the left of each panel show the probability distribution of all identified cold pools. Shading shows the conditional probability distribution at each local phase of the Madden-Julian Oscillation (MJO) as anomalies from the probability of all cold pools. The probabilities are smoothed using a three-point triangular smoothing along MJO phases and the bins of each quantity.

the intensity of the cold pools and daily OLR anomalies. In contrast, Chen et al. (2016) find that the cold pools tend to be the strongest, deepest, and have the longest recovery times during the suppressed phase of the MJO, based on dropsondes and airborne expendable bathythermograph data from science flights during DYNAMO/ AMIE. They attributed this result to the enhanced rain evaporation and dry air entrainment through downdrafts within the drier environment of the MJO suppressed phase that leads to the strongest cold pools, while weaker surface fluxes result in their slow recovery. Based on the cold pools identified at Addu Atoll, Chandra et al. (2018) also suggest that stronger cold pools occur during the MJO suppressed phase.

The apparent disagreement between our and prior studies likely occurs from the differences in how cold pool properties are quantified. Chen et al. (2016) used airborne data to quantify the intensity of cold pools based on the negative buoyancy integrated over the depth of the cold pool, and they estimated the recovery time with surface fluxes. Those airborne measurements were also made on days and locations of convective systems that were of specific interest (i.e., conditional sampling). Their approach measures cold pool properties at an instantaneous time at varying locations around chosen convective systems. In contrast, the approach of de Szoeke et al. (2017) quantifies the properties of cold pools through the continuous temporal evolution of temperature at a fixed location. The estimated recovery time based on surface fluxes in Chen et al. (2016) also does not include the effects of cold pool collisions that can extend the recovery time. These differences make it challenging to compare the

results of this study and de Szoeke et al. (2017) with Chen et al. (2016). However, we speculate that, if an MCS forms, it may generate stronger cold pools during the MJO suppressed phase as found by Chen et al. (2016) and Chandra et al. (2018), but the frequency of MCS formation is also lower during the MJO suppressed phase, which can result in the weakening of cold pools when all cold pools are considered, not just of those around MCSs.

We test this speculation by checking the chance of observing strong cold pools (defined as intensity greater than 2°C) when they occur with MCSs. MCSs are identified using the radars as continuous raining areas that consist of stratiform rain (Sakaeda & Torri, 2022). We find that when a cold pool occurs with an MCS, the chance of it being a strong cold pool is nearly twice as high during the suppressed than enhanced phase of the MJO at the Addu Atoll (not shown). However, the same result is not found at the *Revelle*, which does not fully support our speculation.

Furthermore, the low statistical confidence in our results indicates that a small change in the sampling can lead to different conclusions. For example, the limited eight cases of cold pools examined by Chandra et al. (2018) might not be sufficient to investigate the intraseasonal variability of cold pools. These results highlight the need for more data collection to understand if and how cold pool properties vary with the MJO.

4. Convective Triggering by Cold Pools

Despite the ambiguity in how cold pool properties vary with the MJO, the effectiveness of cold pools on convective triggering may still depend on the MJO. We examine the convective triggering at the identified location of cold pools (in situ triggering) and at a broader range of distances using the scanning radars. This section demonstrates the observed impacts of cold pools on convection development and organization and that those impacts depend on the large-scale environment associated with the MJO.

4.1. In Situ Triggering of Rainfall by Cold Pools

We first apply the approach of de Szoeke et al. (2017) to examine how the evolution of rainfall associated with cold pools depends on the MJO using rain gauges. The rain gauges at Addu Atoll and the *Revelle* capture the increased rainfall during the enhanced phase of the MJO (The black line at the top of Figures 6a and 6b). Within the different phases of the MJO, we then examine the evolution of rainfall with respect to cold pools on a normalized time between the maximum and minimum temperatures (t_{max}, t_{min}) of the identified cold pools (the shadings of Figures 6a and 6b). To emphasize the impact of the cold pools, the average rain rates between 60 and 15 min before t_{max} are also removed within each MJO local phase. Figure 6 shows that cold pools are more effective at triggering rainfall around the enhanced than suppressed phase of the MJO.

We also use CombRet to understand the types of clouds formed by the cold pools at Addu Atoll. All cloud frequencies are shown as normalized anomalies in Figures 6c–6e, which are calculated by removing their average frequencies (about 0.07–0.08) and dividing them by the same averages. On an intraseasonal timescale, as shown by other studies, the frequency of shallow clouds maximizes during the suppressed phase of the MJO, while deeper clouds become more frequent during the enhanced phase of the MJO (Barnes & Houze, 2013; Powell & Houze, 2013).

Figures 6c and 6d confirm the finding of Chandra et al. (2018) that cold pools tend to form cumuli that only reach the mid-troposphere. Shallow clouds become more frequent as the cold pool fronts arrive (i.e., at around t_{max}), followed by the increased frequency of congestus clouds, especially around the MJO enhanced phase. However, Figure 6e shows that those clouds then tend to develop into deep clouds 15–60 min after the passage of the cold pool fronts. We also find that the cold pools have minimal in situ effects on non-precipitating cloud types (cloud base above 3 km, such as cirrus and anvil clouds), and therefore, those cloud types are not shown.

The intraseasonal variability of the effectiveness of the cold pools on the in situ triggering of rainfall and clouds can be attributed to changes in the large-scale environment by the MJO or associated changes in the thermodynamic and dynamic forcing of the cold pools. The top panels of Figure 7 show that, from the MJO suppressed to enhanced phase, the surface temperature cools, water vapor mixing ratio increases, and surface wind speed increases as documented previously (Ruppert & Johnson, 2015; Sobel et al., 2014). The general evolution of these variables relative to cold pools resembles the prior results (Chandra et al., 2018; de Szoeke et al., 2017; Zuidema et al., 2017), but there are some subtle changes with the MJO. For example, as indicated by Figure 5, the temperature evolution of cold pools displays a subtle but not statistically significant variability with the MJO.

The evolution of near-surface moisture and wind speed of the cold pools shows some differences between Addu Atoll and the *Revelle*. At Addu Atoll, the cold pools within the MJO enhanced phase have a slightly greater
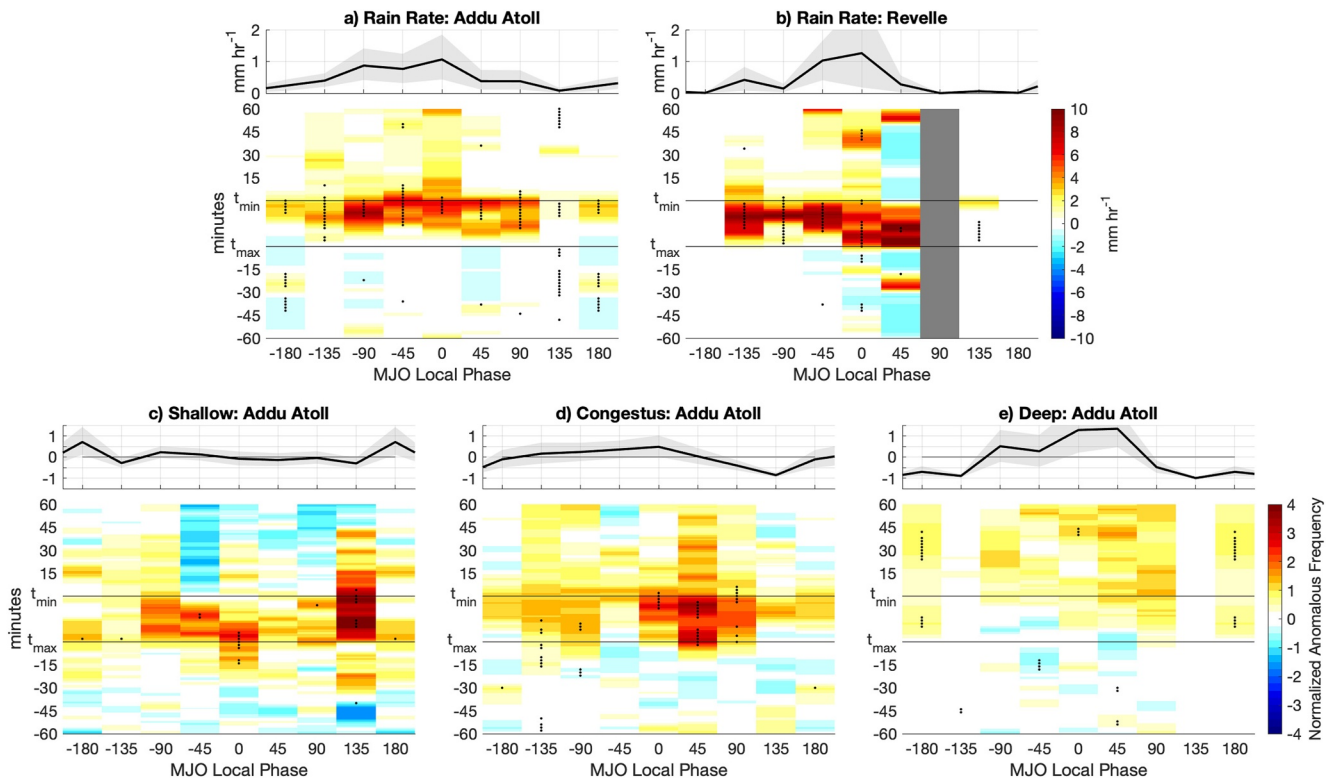
Figure 6. (a and b) The top black lines show the average rain rates from rain gauges at each phase of the Madden-Julian Oscillation (MJO) at Addu Atoll and the *Revelle*. Gray shading shows their 95% confidence interval. Red and blue shadings show rain rates relative to the times of cold pools within each MJO phase, shown as the anomalies from their mean values over 15–60 min before t_{max}. A triangular running average with a 5-min window is applied to smooth the anomalies. Dots show the anomalies that are statistically significantly different from zero at the 95% confidence level. (c–e) Same as panels (a and b), except showing the normalized frequency of shallow, congestus, and deep clouds from CombRet data at Addu Atoll.

increase in water vapor mixing ratio at the edge of cold pool fronts (around t_{max}) and a stronger increase in wind speed along the cold pool fronts (between t_{max} and t_{min}) (Figures 7b and 7c). These results suggest that cold pools provide stronger mechanical and thermodynamic forcing at the boundary layer to trigger convection within the MJO enhanced phase (Torri et al., 2015). At the *Revelle*, the slight increase in water vapor mixing ratio around t_{max} is similarly observed during the MJO enhanced phase, but the timing of such increase shifts to between t_{max} and t_{min} (inside cold pools) during the MJO suppressed phase. The intraseasonal variability in the strength of the wind speed at the cold pool fronts is also less clear at the *Revelle*. These results suggest that the mechanical forcing of cold pools at the *Revelle* does not change significantly with the MJO, but the thermodynamic forcing does. However, the opposite appears at Addu Atoll, where the mechanical forcing of cold pools, rather than their thermodynamic forcing, changes more with the MJO.

The cause of these differences in the near-surface moisture of cold pools (thermodynamic forcing) between the *Revelle* and Addu Atoll is unclear, but we provide some potential explanations. In general, the sub-cloud layer is expected to be more saturated and surface latent heat flux is known to be higher during the MJO enhanced than suppressed phase (de Szoeke et al., 2015; Sobel et al., 2010). Therefore, the increased moisture at the edges of cold pool fronts during the MJO enhanced phase at both locations might be due to the convergence of this moist boundary layer air. In contrast, during the MJO suppressed phase, the increased moisture might appear inside the cold pools at the *Revelle* due to enhanced rain evaporation in the drier environment and surface latent heat flux, which is higher over the ocean. The cause of the difference in surface wind speed between the two locations is also unclear, but we speculate that the presence of the Addu Atoll might weaken the gust front, especially when cold pools tend to be weaker during the MJO suppressed phase.

Despite these differences in the thermodynamic and dynamic forcing of the cold pools at Addu Atoll and the *Revelle*, the cold pools at both locations lead to enhanced rainfall triggering during the MJO enhanced phase. This result could imply that the large-scale environment associated with the MJO has a greater impact on determining
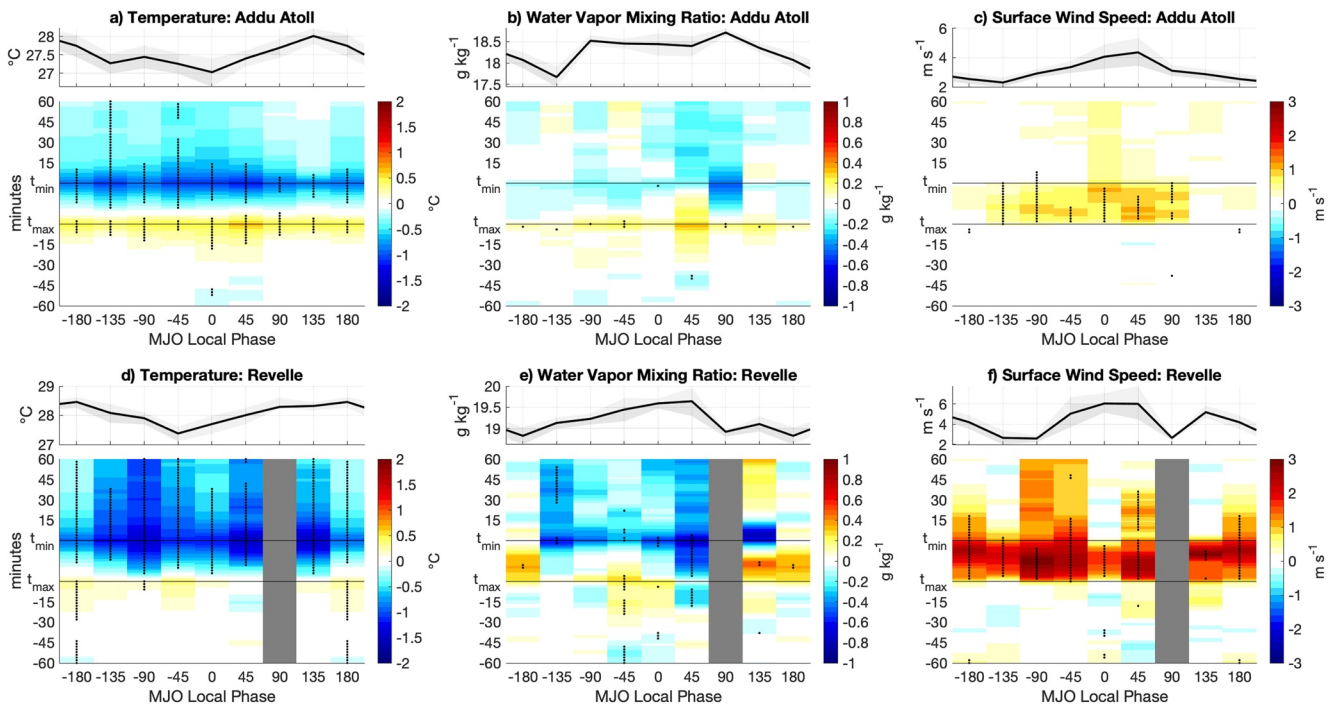
Figure 7. Same as Figure 6 except showing near-surface (a and d) air temperature (°C), (b and e) water vapor mixing ratio (g kg^{-1}), and (c and f) wind speed (m s^{-1}) within each Madden-Julian Oscillation local phase at (top row) Addu Atoll and (bottom row) the *Revelle*.

the effectiveness of cold pools on convection triggering than cold pool properties. For example, the free troposphere is more humid during the MJO enhanced phase (Kiladis et al., 2005; Sakaeda & Torri, 2022). Therefore, we speculate that lifted parcels can sustain their buoyancy and lead to the more frequent triggering of deep convection by cold pools (Feng et al., 2015). However, the presented analysis is limited to the in situ triggering of rainfall, which does not fully demonstrate the role of cold pools on cloud organization.

4.2. Spatio-Temporal Evolution of Rainfall Relative to Cold Pools

To further understand the role of cold pools on cloud organization, this section uses rainfall estimates from scanning radars to examine the evolution of rainfall relative to the cold pools. Figure 8 shows the composite of radar-estimated rainfall as a function of time and distance from the identified cold pools at Addu Atoll and the *Revelle*. The reference time 0 is t_{max}, and the negative and positive minutes indicate the time before and after t_{max}, respectively. The composites are not plotted on the normalized time between t_{max} and t_{min} as in Section 4.1 due to the coarse temporal resolution of radar scans (10–15 min) relative to the duration of cold pools (15–30 min). The rainfall composites with respect to the cold pools are then compared to the same composites relative to randomly selected times within ±3 hr of t_{max} of the composited cold pools. This difference is shown in Figure 8, which highlights the enhancement (positive anomaly) or suppression (negative anomaly) of rainfall associated with cold pools within a similar environment and local time of the day.

Figures 8a and 8b show that rainfall is enhanced around the cold pools over a wide range of distances before and after their occurrence at both Addu Atoll and the *Revelle*. Rainfall anomalies propagate toward cold pools at speeds of 10–20 m s^{-1}, followed by rainfall propagation away from cold pools at a slower range of speeds (3–8 m s^{-1}). The observed average lower tropospheric wind (850 hPa) at the times of identified cold pools is roughly westerly at 5.2 and 5.5 m s^{-1} at Addu Atoll and the *Revelle*, respectively, indicating that the observed speeds of rainfall propagation cannot be explained solely by advection. The typical propagation speed of cold pools in the tropics based on numerical simulations is around 1–3 m s^{-1} (Grant et al., 2018; Torri & Kuang, 2019). Therefore, we suspect that the slower propagation speeds at around 3–8 m s^{-1} correspond to the cold pool propagation speeds that include the Doppler shifting effect by the background wind. Compared with the expected speed associated with observed temperature anomalies (<3°C) (Cotton et al., 2011; Rotunno et al., 1988), the faster propagation
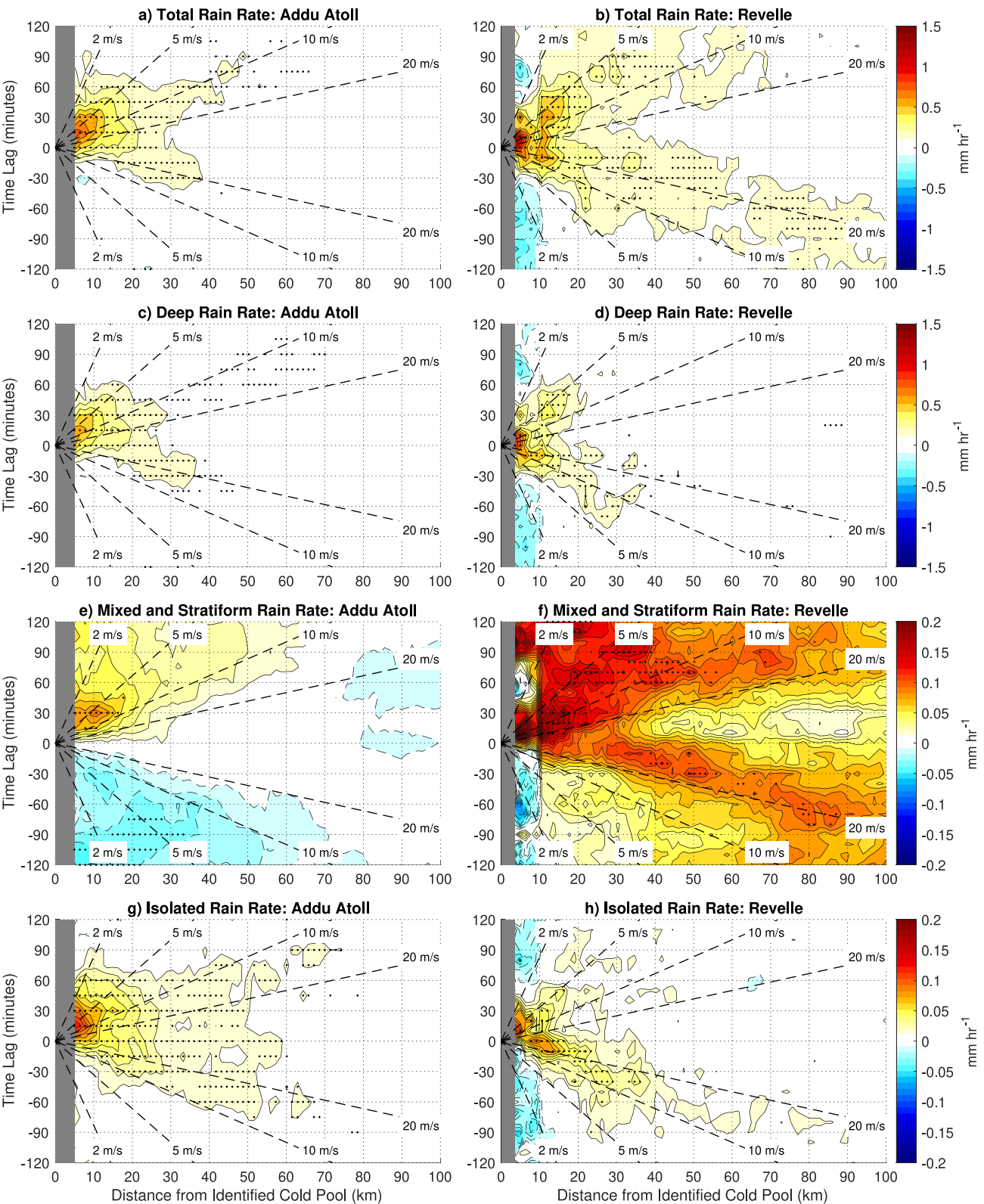
Figure 8. Composites of radar-estimated rain rates relative to the identified cold pools at (left column) Addu Atoll and (right column) the *Revelle*. Positive rain rate anomalies indicate enhancement and negative indicate suppression of rain rate associated with the cold pools (see text for more description), where dots indicate anomalies that are statistically significantly different from zero at the 95% level. Each row shows different types of rain rates: (a and b) total, (c and d) deep convective, (e and f) mixed convective and stratiform, and (g and h) isolated convective rain. Black dashed lines show propagation speeds at 2, 5, 10, and 20 m s^{-1}.

speeds at 10–20 m s^{-1} are too fast to be a density current. Therefore, those faster speeds may be associated with gravity waves or "gust front" waves identified by Tulich and Mapes (2008).

The enhancement of rainfall at the speeds of cold pools (3–8 m s^{-1}) also occurs exclusively after the identified cold pools at Addu Atoll, but not prior to them. This contradicts our expectation to see the "parent convection" that initiates cold pools. If the identified cold pools all propagate at around 3–8 m s^{-1} once formed by their parent convection, then we would expect to see the enhanced rainfall that appears to propagate at those speeds toward the identified location of cold pools. One possible explanation of this result is that the parent convection that initiates the identified cold pools occurs within the close range of the radar where data is unavailable. Especially at Addu Atoll, the cold pools are identified southeast of the radar within the range where rain estimates are unavailable. This means that more data were missing in the 10–20 km distance upstream of cold pools, given that the average lower-tropospheric wind was east-southeastward.

In contrast to Addu Atoll, some enhancement of rainfall prior to the cold pools at the speeds of 3–8 m s^{-1} is seen at the *Revelle* within 8 km from the cold pools. This result further suggests that the signal of parent convection that initiates cold pools is only evident within a short range of distance (<10 km), which was not captured due to the unavailability of data upstream of cold pools at Addu Atoll. After the occurrence of cold pools, the enhancement of deep and isolated convective rain along the speeds of cold pools also only occurs within about 20 km (Figure 8c–d, g–h). These results suggest that cold pools are effective at generating new convection within a short range (<20 km), playing an important role in the clustering and organization of convection as supported by prior studies. For example, Torri and Kuang (2019) find that most cold pools tend to collide in the first 10 min of formation, leading to convection triggering in a short distance. Cheng et al. (2020) and Rowe and Houze (2015) also find that convection initiation by cold pools leads to convective clustering, especially at an early stage of cloud organization.

While cold pools seem to trigger convection in a short distance, rainfall anomalies along the speeds of gravity or gust front waves appear over a wider range of distances, extending to 70 km or beyond. This result suggests that the gravity and gust front waves are the primary driver of the movement of rainfall, as concluded by Grant et al. (2018). Because the parent convection that generates cold pools moves at the speeds of gravity and gust front waves, their signals also appear in Figure 8 even though no significant surface temperature anomalies are expected from gravity waves (Haertel et al., 2001; Tulich & Mapes, 2008). The observed speeds of gravity waves correspond to 5–10 km vertical wavelengths using the observed average Brunt-Väisällä frequency of about 0.012 s^{-1}. If the Doppler-shifting effect by the background flow (∼ 5 m s^{-1}) is removed, they correspond to 3–8 km vertical wavelengths. These vertical wavelengths are likely associated with isolated and stratiform rain (Mapes, 1993).

Figures 8c–8h confirm that the gravity wave propagation speed of total rain is largely attributed to isolated deep convection and stratiform rain in general. However, some differences between Addu Atoll and the *Revelle* appear prior to the cold pools. At Addu Atoll, stratiform rain is suppressed prior to the cold pools, and rainfall anomalies that propagate toward the cold pools are associated with deep and isolated rainfall. In contrast, at the *Revelle*, stratiform rain also propagates toward the cold pool at a fast speed of around 20 m s^{-1}. Despite some differences, stratiform rain is enhanced after the occurrence of cold pools at both locations. This result suggests that the upscale growth and formation of MCSs are more likely after the occurrence of cold pools (Cheng et al., 2020; Rowe & Houze, 2015; Tompkins, 2001a). The enhancement of rainfall at a wider range of speeds due to both cold pools and gravity waves likely results in the formation of convection over a wide range of distances, leading to the organization of convection.

Cold pools are further subdivided into the four phases of the MJO that capture the different states of cloud populations and organization (Sakaeda & Torri, 2022): MJO suppressed-to-growing phase is defined as the MJO local phase angle between −180° and −90° where rainfall begins to increase; growing-to-enhanced phase (−90°–0°) is the state of maximum rainfall; enhanced-to-decaying phase (0°–90°) is the state of slowly decaying rainfall with a high fraction of stratiform-anvil rainfall; and decaying-to-suppressed phase (90°–180°) is when rainfall minimizes again (Figures 3a and 3b).

The evolution of rainfall associated with cold pools shows some sensitivity to the state of the MJO at both Addu Atoll and the *Revelle* (Figure 9). Around the suppressed phase of the MJO (Figures 9a and 9b and 9g and 9h), the enhancement of rainfall following the occurrence of cold pools is minimal or limited to a small range of distances
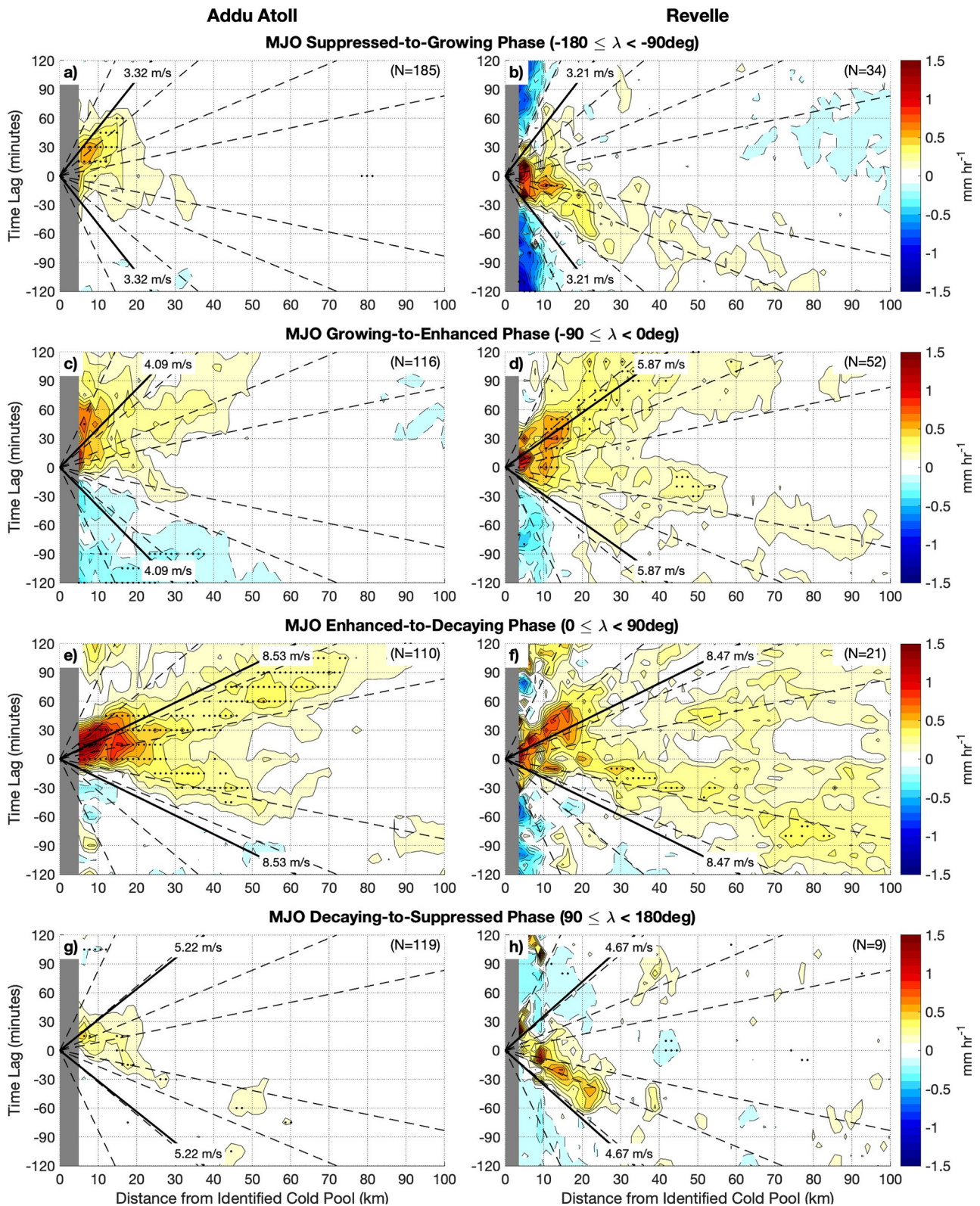
Figure 9. Same as Figure 8, except showing the total rainfall anomalies relative to the cold pools identified during different phases of the Madden-Julian Oscillation (MJO). (a and b) MJO suppressed-to-growing ($-180° \leq \lambda <- = 90°$), (c and d) growing-to-enhanced ($-90° \leq \lambda < 0°$), (e and f) enhanced-to-decaying ($0° \leq \lambda < 90°$), and (g and h) decaying-to-suppressed phase ($90° \leq \lambda < 180°$). Black dashed lines show the same propagation speeds as in Figure 8. Black thick solid lines show the average 850 hPa horizontal wind speed for each set of cold pools. The number of N at the top-right corner of each figure shows the number of composited cold pools.

(within 20 km). In those states of the MJO, rainfall anomalies that propagate toward the cold pools are still present (except Figure 9a) but over a shorter distance. This result indicates that convection is generally short-lived and cold pools are less effective at generating new convection, perhaps due to the drier environment. Around the enhanced phase of the MJO (Figures 9c–9f), cold pools appear to be more effective at generating new rainfall over a wider range of distances.

The propagation speed of rainfall preceding the cold pools also becomes the fastest during the MJO enhanced-to-decaying phase. This fast propagation speed of rainfall is likely caused by the stronger lower-tropospheric wind speed that is observed during the MJO enhanced-to-decaying phase. This phase of the MJO is associated with anomalous lower-tropospheric westerlies that strengthen the westerly background wind over the Indian basin (Seiki & Takayabu, 2007; Sobel et al., 2011). These anomalous lower-tropospheric westerlies also lead to stronger vertical wind shear in the boundary layer and in the free troposphere above (Lin et al., 2004; Sakaeda & Torri, 2022). The average speed of 850 hPa horizontal wind for each phase of the MJO is indicated with the black solid lines in Figure 9. From MJO growing-to-enhanced phase to enhanced-to-decaying phase, 850 hPa horizontal wind speed increases to about 2.5–4.5 m s^{-1}, which corresponds to a similar amount of increase in rainfall propagation speed. In addition, the enhancement of rainfall associated with cold pools within 20 km is also strongest during the MJO enhanced-to-decaying phase.

These results allow us to infer the role of cold pools on cloud organization associated with the different phases of the MJO that is documented in Sakaeda and Torri (2022). Their study finds that the number of deep convective cells maximizes during the MJO growing-to-enhanced phase, contributing to the maximum rainfall shown in Figures 3a and 3b. However, deep convective cells become least randomly distributed during the enhanced-to-decaying phase of the MJO when the number of deep convective cells begins to decrease. This is the MJO phase where the cold pools are also found to have the strongest enhancement of subsequent rain over a wide range of distances (Figure 9). During the growing-to-enhanced phase of the MJO, when the environmental moisture is at its peak, there is a greater number of deep convective cells, but their occurrence may be less associated with cold pools. Sakaeda and Torri (2022) speculated that the high environmental moisture allows convection to form more randomly due to the favorable environment for convection to develop and sustain. This does not mean that cold pools are less effective at generating convection during the growing-to-enhanced phase of the MJO. Rather, we suggest that any perturbation (not necessarily from cold pools) can lead to convection development at this state of the MJO. This is supported by Cheng et al. (2020), who find that the removal of all perturbations in the boundary layer temperature suppresses cloud organization during its early stage.

In contrast, during the MJO enhanced-to-decaying phase, when the environmental humidity decreases and vertical wind shear increases, mechanical and thermodynamic triggering by cold pools might be more important for initiating new convection, leading to the state of least random distribution of convection. This hypothesis is supported by Figure 9, which shows that the occurrence of cold pools is more strongly associated with rainfall surrounding it during the MJO enhanced-to-decaying phase. This hypothesis contradicts the finding of Cheng et al. (2020), who suggest that cold pools are less relevant to cloud organization when there is widespread stratiform rain. Their finding comes from the sensitivity experiments of a 2-day rain event during 15–17 October of DYNAMO/AMIE at Addu Atoll, which occurred during the MJO developing phase when the vertical wind shear is relatively weak (Sakaeda & Torri, 2022). Therefore, we further examine the role of vertical wind shear on convective initiation by cold pools.

The initiation of new convective clouds by cold pools has been hypothesized to be enhanced by the interactions with boundary layer vertical wind shear (Rotunno et al., 1988; Schlemmer & Hohenegger, 2014; Weisman & Rotunno, 2004). To identify the role of their interactions, the radar domain is separated into up-shear and down-shear halves based on the direction of boundary-layer (900–1,000 hPa) shear. The times with a shear magnitude smaller than one standard deviation within the entire DYNAMO period is considered weak shear. Figure 10 illustrates that the evolution of rainfall around cold pools shows distinct behaviors between up-shear and down-shear domains. Within the up-shear domain, rainfall mainly propagates toward the cold pools, while rainfall propagates away from cold pools in the down-shear domain.

Furthermore, the slower propagation speed of rainfall (3–8 m s^{-1}) that we attributed to cold pools is only seen within the down-shear domain. This result suggests that cold pools tend to predominantly trigger new rainfall within the down-shear domain (Rotunno et al., 1988). While we separate the radar domain based on the
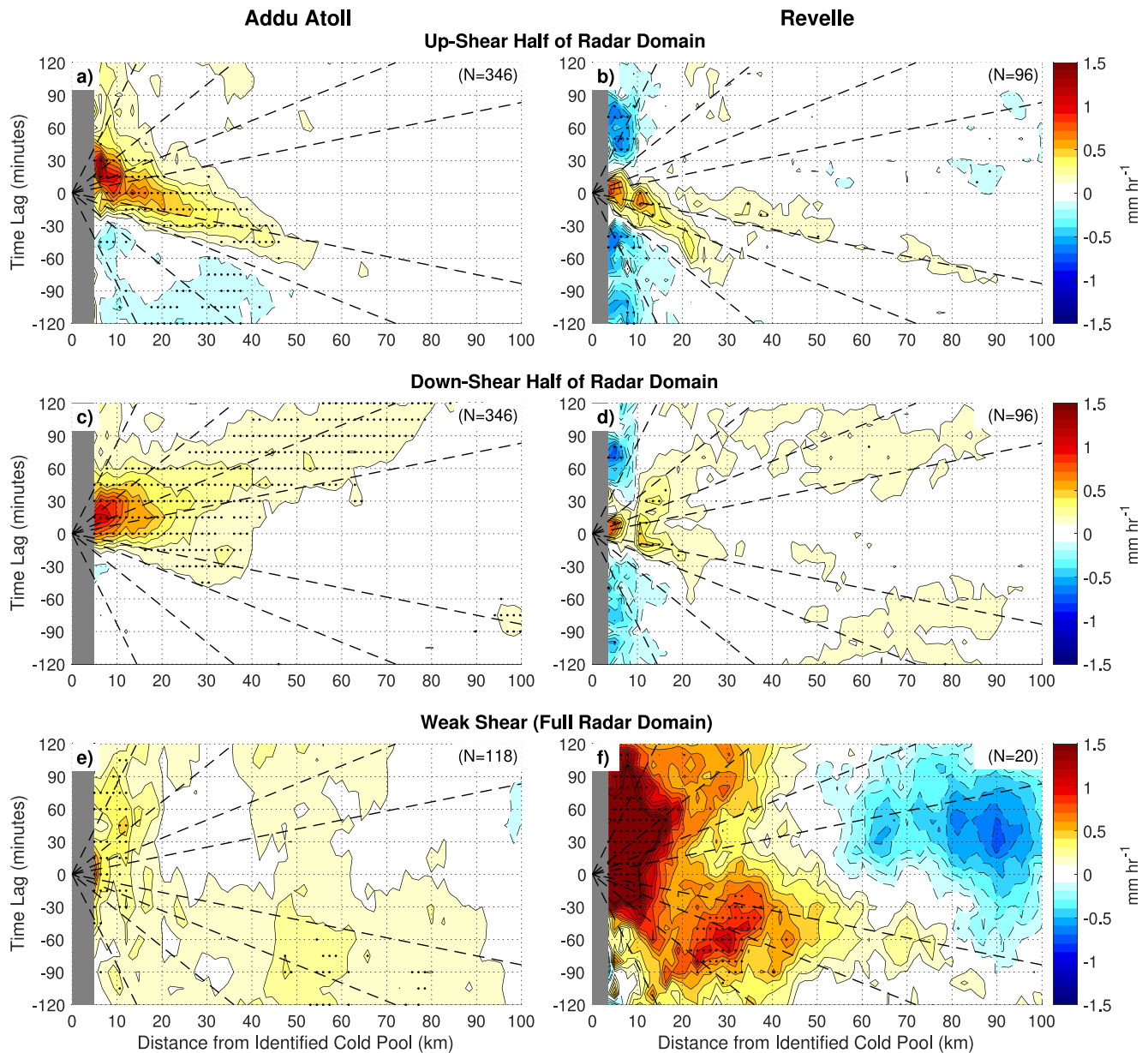
Figure 10. Same as Figure 8, except showing the total rainfall anomalies within the (top) up-shear and (middle) down-shear half of the radar domain based on the 900–1,000-hPa vertical shear direction of the horizontal wind at the times of cold pools. Days with a vertical wind shear of less than one standard deviation during the entire DYNAMO period are considered weak shear. (c) Composites of full radar domain rainfall anomalies during cold pools with weak shear.

directions of boundary layer shear, the directions and strength of boundary layer shear are highly correlated with lower-tropospheric (e.g., 850 hPa) wind. Therefore, the difference in the preferred direction of rainfall at the faster gravity wave speeds may be due to the Doppler-shifting effect again. At Addu Atoll, weak shear is not associated with significant rainfall enhancement, while large rainfall enhancement is associated with the cold pools at the *Revelle* on weak shear conditions. However, the sample size of those at the *Revelle* is too small (only 20) to interpret the results with much confidence. These results suggest that the presence of strong vertical wind shear during the enhanced-to-decaying phase of the MJO is also important for convection triggering by cold pools (Sakaeda & Torri, 2022).
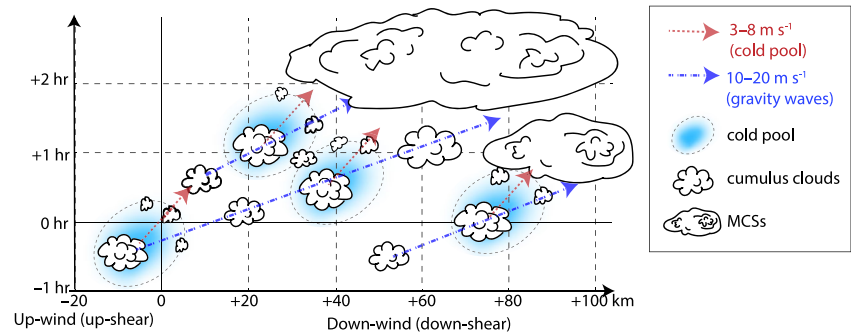
Figure 11. Schematic illustration of convection triggering by cold pools and gravity waves. Arrows show the propagation speeds of (red) 3–8 m s^{-1} and (blue) 10–20 m s^{-1}, corresponding to cold pools and gravity waves, respectively. Blue circular shadings show cold pools. Reference time 0 and distance 0 indicate the time of an identified cold pool at a fixed point in our method. Positive distances indicate the direction of lower-tropospheric wind or boundary-layer vertical wind shear, while negative distances indicate the opposite direction. Positive and negative times indicate the times after and before the time of an identified cold pool at the reference point. Convection triggering by gravity waves occurs over a long range of distances (beyond 50 km) in the down-wind (down-shear) direction while cold pools initiate convection within the range of 10–20 km. Their interactions can lead to cloud organization or the formation of MCSs.

5. Conclusions

The main objectives of this study are to examine the intraseasonal variability in the properties of cold pools and their roles in supporting cloud organization using observations collected during the DYNAMO/AMIE field campaign. This study adds further observational evidence that cold pools are effective at generating new convection. This was evident by the enhancement of rainfall following the occurrence of cold pools that propagate at their expected speed (3–8 m s^{-1}, including the Doppler-shifting effect). However, the effective areas of new convection triggering are limited to 20 km from the identified location of cold pools.

Composites of rainfall with respect to cold pools also revealed that rainfall propagates toward and away from the cold pools at faster speeds (10–20 m s^{-1}) that correspond to gravity wave speeds. The appearance of these speeds suggests that gravity waves play a dominant role in the propagation of convective systems, in agreement with prior studies (Fovell et al., 2006; Grant et al., 2018; Mapes, 1993). Such convective systems that propagate at the speed of gravity waves generate cold pools that are detected by our algorithm. While those cold pools generate new convection within the limited distance, gravity waves allow convection to continue propagating at a faster speed. The interactions of convection triggering and movement through cold pools and gravity waves may help the clustering (organization) of convection as illustrated in Figure 11. This was evident by increased stratiform rain fraction over a broader domain (100 km range) following the occurrence of cold pools as well.

The effectiveness of generating new convection by cold pools is also dependent on the state of the MJO. Cold pools are more effective at generating new convection during the enhanced phase of the MJO. This more-effective convection generation appears to be supported mainly by the large-scale environment since no statistically significant change in cold pool properties is found with the MJO. The environment is more humid during the MJO enhanced phase, helping to sustain the buoyancy of lifted air parcels (Feng et al., 2015; Romps & Kuang, 2010; Tompkins, 2001b). However, rainfall is most enhanced around the cold pools during the enhanced-to-decaying phase of the MJO when the environment begins to dry while vertical wind shear maximizes (Sakaeda & Torri, 2022). This evidence supports the hypothesis by Sakaeda and Torri (2022) that cold pools and their interaction with vertical wind shear become more important to clustering convection as the drier environment becomes less supportive of convection development from other random weak perturbations. This study also showed that the convection triggering by cold pools occurs predominantly in the direction of the boundary-layer vertical wind shear. The strength of boundary-layer shear is also highly associated with the lower-tropospheric wind, affecting the speed of gravity waves as well. Therefore, the combined effect of boundary-layer shear and associated lower-tropospheric wind enhance convection triggering by cold pools and a wider spread of convection by gravity waves, supporting the organization of clouds (Figure 11).

While it is difficult to detect convection triggering by cold pools in observations, the unique set of DYNAMO/AMIE observations provided new insights into the effect of cold pools on cloud organization. This work demonstrates a new use of observations to study the effects of cold pools on cloud organization for future fieldwork. For example, while this study was limited to identifying cold pools at one station near a scanning radar, a strategic deployment of a network of surface measurement stations around a radar could better identify the propagation and evolution of cold pool properties and their effect on cloud development. The applied diagnostics within this study can also be applied to numerical simulations for their comparison with observational analyses. Our study suggests that the interactions among cold pools, gravity waves, and the large-scale environment lead to varying degrees of cloud organization. More details on their relative roles could be understood through the application of our diagnostics in numerical experiments.

Data Availability Statement

The DYNAMO/AMIE data used in this work were obtained from DYNAMO Legacy website (https://orca.atmos.washington.edu/dynamo_legacy/) (Johnson et al., 2018; Rutledge et al., 2018). The PNNL Combret data is available from DOE Atmospheric Radiation Measurement (https://www.arm.gov/data/data-sources/cldradheatcombret-71) (Feng, 2014). NOAA Interpolated OLR is available from NOAA Physical Sciences Laboratory website (https://psl.noaa.gov/data/gridded/data.olrcdr.interp.html) (Liebmann & Smith, 1996). The identified cold pools analyzed in this study are made available at http://nsakaeda.oucreate.com/data-and-products/.

References

Adames, Á. F., & Wallace, J. M. (2015). Three-dimensional structure and evolution of the moisture field in the mjo. *Journal of the Atmospheric Sciences*, *72*(10), 3733–3754. https://doi.org/10.1175/JAS-D-15-0003.1

Barnes, H. C., & Houze, R. A. (2013). The precipitating cloud population of the Madden-Julian Oscillation over the Indian and West Pacific oceans. *Journal of Geophysical Research: Atmospheres*, *118*(13), 6996–7023. https://doi.org/10.1002/jgrd.50375

Böing, S. J., Jonker, H. J. J., Siebesma, A. P., & Grabowski, W. W. (2012). Influence of the subcloud layer on the development of a deep convective ensemble. *Journal of the Atmospheric Sciences*, *69*(9), 2682–2698. https://doi.org/10.1175/JAS-D-11-0317.1

Chandra, A. S., Zuidema, P., Krueger, S., Kochanski, A., de Szoeke, S. P., & Zhang, J. (2018). Moisture distributions in tropical cold pools from equatorial Indian Ocean observations and cloud-resolving simulations. *Journal of Geophysical Research: Atmospheres*, *123*(20), 11445–11465. https://doi.org/10.1029/2018JD028634

Chen, S. S., Kerns, B. W., Guy, N., Jorgensen, D. P., Delano, J., Viltard, N., et al. (2016). Aircraft observations of dry air, the ITCZ, convective cloud systems, and cold pools in MJO during dynamo. *Bulletin of the American Meteorological Society*, *97*(3), 405–423. https://doi.org/10.1175/BAMS-D-13-00196.1

Cheng, W.-Y., Kim, D., Rowe, A., Moon, Y., & Wang, S. (2020). Mechanisms of convective clustering during a 2-day rain event in AMIE/DYNAMO. *Journal of Advances in Modeling Earth Systems*, *12*(3), e2019MS001907. https://doi.org/10.1029/2019ms001907

Ciesielski, P. E., & Johnson, R. H. (2021). Small island effects in dynamo and their impact on large-scale budget analyses. *Journal of Applied Meteorology and Climatology*, *60*(4), 577–594. https://doi.org/10.1175/JAMC-D-20-0238.1

Ciesielski, P. E., Yu, H., Johnson, R. H., Yoneyama, K., Katsumata, M., Long, C. N., et al. (2014). Quality-controlled upper-air sounding dataset for DYNAMO/CINDY/AMIE: Development and corrections. *Journal of Atmospheric and Oceanic Technology*, *31*(4), 741–764. https://doi.org/10.1175/jtech-d-13-00165.1

Cotton, W. R., Bryan, G., van den Heever, S. C., Cotton, W., & van den Heever, S. (2011). Chapter 8 - Cumulonimbus clouds and severe convective storms. In *International geophysics* (Vol. 99, pp. 315–454). Academic Press. https://doi.org/10.1016/S0074-6142(10)09914-6

de Szoeke, S. P., Edson, J. B., Marion, J. R., Fairall, C. W., & Bariteau, L. (2015). The MJO and air–sea interaction in toga coare and dynamo. *Journal of Climate*, *28*(2), 597–622. https://doi.org/10.1175/JCLI-D-14-00477.1

de Szoeke, S. P., Skyllingstad, E. D., Zuidema, P., & Chandra, A. S. (2017). Cold pools and their influence on the tropical marine boundary layer. *Journal of the Atmospheric Sciences*, *74*(4), 1149–1168. https://doi.org/10.1175/JAS-D-16-0264.1

Dolan, B., Hein, P., Rutledge, S., & Powell, S. (2017). DYNAMO legacy rainfall products. Retrieved from https://orca.atmos.washington.edu/dynamo_legacy/resources/documents/readme/radar/radar_spolka_readme.pdf

Falk, N. M., & van den Heever, S. C. (2023). Environmental modulation of mechanical and thermodynamic forcing from cold pool collisions. *Journal of the Atmospheric Sciences*, *80*(2), 375–395. https://doi.org/10.1175/JAS-D-22-0020.1

Feng, Z. (2014). Combined retrieval, microphysical retrievals heating rates (CLDRADHEATCOMBRET) [Dataset]. https://doi.org/10.5439/1169498

Feng, Z., Hagos, S., Rowe, A. K., Burleyson, C. D., Martini, M. N., & de Szoeke, S. P. (2015). Mechanisms of convective cloud organization by cold pools over tropical warm ocean during the AMIE/DYNAMO field campaign. *Journal of Advances in Modeling Earth Systems*, *7*(2), 1942–2466. https://doi.org/10.1002/2014ms000384

Feng, Z., McFarlane, S. A., Schumacher, C., Ellis, S., Comstock, J., & Bharadwaj, N. (2014). Constructing a merged cloud–precipitation radar dataset for tropical convective clouds during the DYNAMO/AMIE experiment at Addu Atoll. *Journal of Atmospheric and Oceanic Technology*, *31*(5), 1021–1042. https://doi.org/10.1175/jtech-d-13-00132.1

Fovell, R. G., Mullendore, G. L., & Kim, S.-H. (2006). Discrete propagation in numerically simulated nocturnal squall lines. *Monthly Weather Review*, *134*(12), 3735–3752. https://doi.org/10.1175/MWR3268.1

Garg, P., Nesbitt, S. W., Lang, T. J., & Priftis, G. (2021). Diurnal cycle of tropical oceanic mesoscale cold pools. *Journal of Climate*, *34*(23), 9305–9326. https://doi.org/10.1175/JCLI-D-20-0909.1

Grant, L. D., Lane, T. P., & van den Heever, S. C. (2018). The role of cold pools in tropical oceanic convective systems. *Journal of the Atmospheric Sciences*, *75*(8), 2615–2634. https://doi.org/10.1175/JAS-D-17-0352.1

Haertel, P. T., Johnson, R. H., & Tulich, S. N. (2001). Some simple simulations of thunderstorm outflows. *Journal of the Atmospheric Sciences*, *58*(5), 504–516. https://doi.org/10.1175/1520-0469(2001)058⟨0504:SSSOTO⟩2.0.CO;2

Johnson, R., Schubert, W., Taft, R., & Ciesielski, P. (2018). DYNAMO atmospheric sounding data and products [Dataset]. UCAR Earth Observing Laboratory. Retrieved from https://orca.atmos.washington.edu/dynamo_legacy/resources/documents/readme/soundings/soundings_readme.pdf

Khairoutdinov, M., & Randall, D. (2006). High-resolution simulation of shallow-to-deep convection transition over land. *Journal of the Atmospheric Sciences*, *63*(12), 3421–3436. https://doi.org/10.1175/JAS3810.1

Kiladis, G. N., Straub, K. H., & Haertel, P. T. (2005). Zonal and vertical structure of the Madden–Julian oscillation. *Journal of the Atmospheric Sciences*, *62*(8), 2790–2809. https://doi.org/10.1175/JAS3520.1

Liebmann, B., & Smith, C. A. (1996). Description of a complete (interpolated) outgoing long-wave radiation dataset [Dataset]. Bulletin America Meteorology Social, *77*, 1275–1277. Retrieved from https://psl.noaa.gov/data/gridded/data.olrcdr.interp.html

Lin, J., Mapes, B., Zhang, M., & Newman, M. (2004). Stratiform precipitation, vertical heating profiles, and the Madden–Julian oscillation. *Journal of the Atmospheric Sciences*, *61*(3), 296–309.

Mapes, B. (1993). Gregarious tropical convection. *Journal of the Atmospheric Sciences*, *50*(13), 2026–2037. https://doi.org/10.1175/1520-0469(1993)050⟨2026:GTC⟩2.0.CO;2

Meyer, B., & Haerter, J. O. (2020). Mechanical forcing of convection by cold pools: Collisions and energy scaling. *Journal of Advances in Modeling Earth Systems*, *12*(11), e2020MS002281. https://doi.org/10.1029/2020MS002281

Moncrieff, M. W. (2019). Toward a dynamical foundation for organized convection parameterization in GCMS. *Geophysical Research Letters*, *46*(23), 14103–14108. https://doi.org/10.1029/2019gl085316

Powell, S. W. (2016). Updraft buoyancy within and moistening by cumulonimbi prior to MJO convective onset in a regional model. *Journal of the Atmospheric Sciences*, *73*(7), 2913–2934. https://doi.org/10.1175/jas-d-15-0326.1

Powell, S. W., & Houze, R. A. (2013). The cloud population and onset of the Madden-Julian Oscillation over the Indian Ocean during DYNAMO-AMIE. *Journal of Geophysical Research: Atmospheres*, *118*(21), 11979–11995. https://doi.org/10.1002/2013JD020421

Powell, S. W., Robert, A., Houze, J., & Brodzik, S. R. (2016). Rainfall-type categorization of radar echoes using polar coordinate reflectivity data. *Journal of Atmospheric and Oceanic Technology*, *33*(3), 523–538. https://doi.org/10.1175/jtech-d-15-0135.1

Retsch, M. H., Jakob, C., & Singh, M. S. (2020). Assessing convective organization in tropical radar observations. *Journal of Geophysical Research: Atmospheres*, *125*(7), e2019JD031801. https://doi.org/10.1029/2019JD031801

Romps, D. M., & Kuang, Z. (2010). Nature versus nurture in shallow convection. *Journal of the Atmospheric Sciences*, *67*(5), 1655–1666. https://doi.org/10.1175/2009JAS3307.1

Rotunno, R., Klemp, J. B., & Weisman, M. L. (1988). A theory for strong, long-lived squall lines. *Journal of the Atmospheric Sciences*, *45*(3), 463–485. https://doi.org/10.1175/1520-0469(1988)045⟨0463:ATFSLL⟩2.0.CO;2

Rowe, A. K., & Houze, R. A. (2015). Cloud organization and growth during the transition from suppressed to active mjo conditions. *Journal of Geophysical Research: Atmospheres*, *120*(19), 2169–8996. https://doi.org/10.1002/2014jd022948

Ruppert, J. H., & Johnson, R. H. (2015). Diurnally modulated cumulus moistening in the preonset stage of the Madden–Julian oscillation during DYNAMO. *Journal of the Atmospheric Sciences*, *72*(4), 1622–1647. https://doi.org/10.1175/jas-d-14-0218.1

Rutledge, S., Hein, P., Dolan, B., Powell, S., & Brodzik, S. (2018). NCAR S-polka radar data: DYNAMO legacy data products [Dataset]. UCAR Earth Observing Laboratory. Retrieved from https://orca.atmos.washington.edu/dynamo_legacy/resources/documents/readme/radar/radar_spolka_readme.pdf

Sakaeda, N., Powell, S. W., Dias, J., & Kiladis, G. N. (2018). The diurnal variability of precipitating cloud populations during dynamo. *Journal of the Atmospheric Sciences*, *75*(4), 1307–1326. https://doi.org/10.1175/jas-d-17-0312.1

Sakaeda, N., & Torri, G. (2022). The behaviors of intraseasonal cloud organization during DYNAMO/AMIE. *Journal of Geophysical Research: Atmospheres*, *127*(7), e2021JD035749. https://doi.org/10.1029/2021JD035749

Schlemmer, L., & Hohenegger, C. (2014). The formation of wider and deeper clouds as a result of cold-pool dynamics. *Journal of the Atmospheric Sciences*, *71*(8), 2842–2858. https://doi.org/10.1175/JAS-D-13-0170.1

Seiki, A., & Takayabu, Y. N. (2007). Westerly wind bursts and their relationship with intraseasonal variations and ENSO. Part I: Statistics. *Monthly Weather Review*, *135*(10), 3325–3345. https://doi.org/10.1175/MWR3477.1

Sobel, A. H., Burleyson, C. D., & Yuter, S. E. (2011). Rain on small tropical islands. *Journal of Geophysical Research*, *116*(D8), D08102. https://doi.org/10.1029/2010jd014695

Sobel, A. H., Maloney, E. D., Bellon, G., & Frierson, D. M. (2010). Surface fluxes and tropical intraseasonal variability: A reassessment. *Journal of Advances in Modeling Earth Systems*, *2*(1), 2. https://doi.org/10.3894/JAMES.2010.2.2

Sobel, A. H., Wang, S., & Kim, D. (2014). Moist static energy budget of the MJO during DYNAMO. *Journal of the Atmospheric Sciences*, *71*(11), 4276–4291. https://doi.org/10.1175/jas-d-14-0052.1

Thompson, E. J., Rutledge, S. A., Dolan, B., Thurai, M., & Chandrasekar, V. (2018). Dual-polarization radar rainfall estimation over tropical oceans. *Journal of Applied Meteorology and Climatology*, *57*(3), 755–775. https://doi.org/10.1175/JAMC-D-17-0160.1

Tobin, I., Bony, S., & Roca, R. (2012). Observational evidence for relationships between the degree of aggregation of deep convection, water vapor, surface fluxes, and radiation. *Journal of Climate*, *25*(20), 6885–6904. https://doi.org/10.1175/jcli-d-11-00258.1

Tompkins, A. M. (2001a). Organization of tropical convection in low vertical wind shears: The role of cold pools. *Journal of the Atmospheric Sciences*, *58*(13), 1650–1672. https://doi.org/10.1175/1520-0469(2001)058<1650:ootcil>2.0.co;2

Tompkins, A. M. (2001b). Organization of tropical convection in low vertical wind shears: The role of water vapor. *Journal of the Atmospheric Sciences*, *58*(6), 529–545. https://doi.org/10.1175/1520-0469(2001)058<0529:ootcil>2.0.co;2

Tompkins, A. M., & Semie, A. G. (2017). Organization of tropical convection in low vertical wind shears: Role of updraft entrainment. *Journal of Advances in Modeling Earth Systems*, *9*(2), 1046–1068. https://doi.org/10.1002/2016ms000802

Torri, G., & Kuang, Z. (2019). On cold pool collisions in tropical boundary layers. *Geophysical Research Letters*, *46*(1), 399–407. https://doi.org/10.1029/2018gl080501

Torri, G., Kuang, Z., & Tian, Y. (2015). Mechanisms for convection triggering by cold pools. *Geophysical Research Letters*, *42*(6), 1943–1950. https://doi.org/10.1002/2015gl063227

Tulich, S. N., & Mapes, B. E. (2008). Multiscale convective wave disturbances in the tropics: Insights from a two-dimensional cloud-resolving model. *Journal of the Atmospheric Sciences*, *65*(1), 140–155. https://doi.org/10.1175/2007jas2353.1

Weisman, M. L., & Rotunno, R. (2004). A theory for strong long-lived squall lines" revisited. *Journal of the Atmospheric Sciences*, *61*(4), 361–382. https://doi.org/10.1175/1520-0469(2004)061⟨0361:ATFSLS⟩2.0.CO;2

Wheeler, M. C., & Kiladis, G. (1999). Convectively-coupled equatorial waves: Analysis of clouds in the wavenumber-frequency domain. *Journal of the Atmospheric Sciences*, *56*(3), 374–399. https://doi.org/10.1175/1520-0469(1999)056<0374:ccewao>2.0.co;2

Xu, W., & Rutledge, S. A. (2014). Convective characteristics of the Madden–Julian Oscillation over the central Indian ocean observed by ship-borne radar during DYNAMO. *Journal of the Atmospheric Sciences*, *71*(8), 2859–2877. https://doi.org/10.1175/jas-d-13-0372.1

Xu, W., & Rutledge, S. A. (2015). Morphology, intensity, and rainfall production of MJO convection: Observations from DYNAMO shipborne radar and TRMM. *Journal of the Atmospheric Sciences*, *72*(2), 623–640. https://doi.org/10.1175/jas-d-14-0130.1

Yang, Q., Majda, A. J., & Moncrieff, M. W. (2019). Upscale impact of mesoscale convective systems and its parameterization in an idealized GCM for an MJO analog above the equator. *Journal of the Atmospheric Sciences*, *76*(3), 865–892. https://doi.org/10.1175/JAS-D-18-0260.1

Yoneyama, K., Zhang, C., & Long, C. N. (2013). Tracking pulses of the Madden-Julian oscillation. *Bulletin America Meteorology Social*, *94*(12), 1871–1891. https://doi.org/10.1175/bams-d-12-00157.1

Zuidema, P., Torri, G., Muller, C., & Chandra, A. (2017). A survey of precipitation-induced atmospheric cold pools over oceans and their interactions with the larger-scale environment. *Surveys in Geophysics*, *38*(6), 1283–1305. https://doi.org/10.1007/s10712-017-9447-x